Nanoscale

Cite this: *Nanoscale*, 2012, **4**, 3635

www.rsc.org/nanoscale

COMMUNICATION

An electrically controlled quantum dot based spin current injector

Szabolcs Csonka,[a] Ireneusz Weymann*[b] and Gergely Zarand[cd]

Received 20th February 2012, Accepted 6th April 2012
DOI: 10.1039/c2nr30399j

We present a proposal for a fully electrically controllable quantum dot based spin current injector. The device consists of a quantum dot that is strongly coupled to a ferromagnetic electrode on one side and weakly coupled to a nonmagnetic electrode on the other side. The presence of the ferromagnetic electrode results in an exchange field that splits the dot level. We show that this exchange-induced splitting can lead to almost full spin polarization of the current flowing through the device. Moreover, we also demonstrate that the sign of polarization can be changed by the gate or the bias voltage within a switching time in the nanosecond range. Thus, the proposed device can operate as an electrically controlled, rapidly switchable spin current source, which can be realized in various state-of-the-art nanostructures.

Spin injection is a central problem in the field of spintronics and the improvement of its efficiency and its control enhances the performance of spin based devices. Most common ferromagnetic electrodes are used as sources of spin polarization, directly injecting spins from a ferromagnet into a connected device.[1] However, the spin injection strongly depends on the ferromagnetic–normal interface: issues with material and problems, such as conductance mismatch,[2,3] make the realization of these boundaries technologically challenging. As an interface between the ferromagnet and the normal part, tunnel barriers are widely used.[4] The polarization of the injected spin current is then limited by the polarization of the tunneling electrons, which—for a typical ferromagnet—is in the range of 30–40%.[5] Another drawback of this configuration is that the sign of the current spin polarization can only be changed by rotating the magnetization of the ferromagnet, *e.g.*, by applying an external magnetic field. Therefore, the spin polarization can be switched only relatively slowly and, in many cases, the application of a local magnetic field is needed.

In this paper, we consider a device with a different geometry, where the conventional tunnel barrier is replaced by a quantum dot (QD) coupled to a ferromagnetic (F) and a normal (N) lead (F/QD//N geometry), see Fig. 1a. We focus on the case where the coupling to the ferromagnet is strong, while the coupling to the normal metal is relatively weak. Based on accurate numerical renormalization group calculations (NRG) we show that, in this instance, the performance of the spin injection in such a quantum dot interface is greatly improved: first, the dot acts as a *spin current amplifier*, *i.e.*, the spin polarization of the injected current highly exceeds that of the

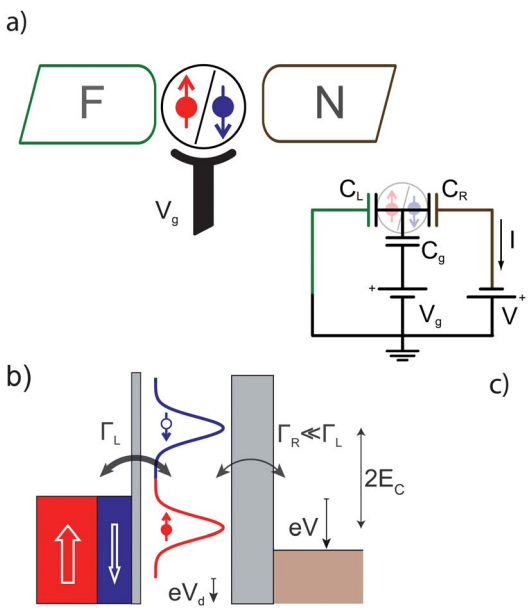

Fig. 1 (a) Device geometry: a quantum dot hosting an odd number of electrons is placed at the interface of a ferromagnet (F) and normal contact (N). The ground state spin of the dot (down or up) determines the spin polarization of the current. (b) An energy diagram of the device: the dot is strongly coupled to the ferromagnetic lead (Γ_L) and weakly coupled to the normal lead (Γ_R). The ferromagnet-induced exchange field strongly polarizes the two resonance peaks of the dot. For the situation shown, the occupied (lower) Hubbard peak is spin-up polarized. The spin polarization of the current is generated by the polarization of the local density of states in the bias window. V is the applied bias voltage and E_C is the charging energy. (c) A classical circuit diagram of the device: the quantum dot is capacitively coupled to the ferromagnetic and normal leads and to the gate electrode with C_L, C_R and C_g, respectively. The gate voltage (V_g) allows modification of the level position. Due to the capacitance values, the applied bias voltage (V) also shifts the dot level downwards, similar to the gate voltage, with a value of $eV_d = -eVC_R/C$, where $C = C_L + C_R + C_g$.

[a]*Department of Physics, Budapest University of Technology and Economics, Budafoki ut 8, 1111 Budapest, Hungary*
[b]*Department of Physics, Adam Mickiewicz University, Poland, 61-614 Poznań. E-mail: weymann@amu.edu.pl*
[c]*Dahlem Center, Freie Universität Berlin, Fachbereich Physik, Germany, Arnimallee 14, 14195 Berlin*
[d]*MTA-BME Quantum Phases Lendulet Research Group, Budapest University of Technology and Economics, Budafoki ut 8, 1111 Budapest, Hungary*

ferromagnetic electrode and may even approach unity. Second, the polarization of the injected spin current becomes *tunable* by *purely electric means*, either by sweeping the gate voltage or simply by changing the applied bias voltage. Both ways enable extremely fast (~1 GHz) spin polarization switching. In this context, we discuss two geometries of our spin injection device. In the first, *three-terminal* device, we control the spin polarization by a gate voltage, while in the second, a *two-terminal* set-up, only the bias voltage is used for control. While the former geometry may be more relevant for semiconducting quantum dots, the latter is more suitable for molecular spintronics applications.

The principle of operation of the proposed spin polarization amplifier is based on the ferromagnetic exchange field induced level renormalization of the dot. When a quantum dot is coupled to external leads and the number of electrons on the dot is odd, strong electronic correlations can give rise to the spin formation and also to the Kondo effect.[6,7] In the case of ferromagnetic leads, quantum fluctuations renormalize the position of the dot levels differently for each spin direction due to the different spin-up and spin-down tunneling rates. This effective exchange field then splits the dot levels and suppresses the Kondo resonance.[8–10] An important effect of the exchange field induced splitting is that the ground state as well as the local density of states of the dot become highly spin polarized. This is, in fact, the major ingredient of the efficient spin polarization amplification discussed here: due to the exchange splitting of the correlated state, the quantum dot will be able to offer spin current polarizations much higher than the ferromagnet itself. The second key ingredient is the asymmetry between the left and right contacts: the coupling to the ferromagnet should be larger than the coupling to the non-magnetic material to assure that only highly spin polarized states carry the current in the transport window associated with the bias voltages. With more symmetrical couplings, one can still operate the device as an ultra-fast spin current injector, but polarizations will be reduced.

The proposed F/QD//N structure is quite generic and our concept can be realized in various types of nanostructures using state-of-the-art nanotechnology. The basic ingredient, *i.e.*, the ferromagnetic contact induced local exchange field,[8,11] has already been demonstrated experimentally in F/QD/F devices, where the QD was defined using fullerene molecules,[10] self-assembled semiconductor nanocrystals[12] or carbon nanotubes.[13,14] Very recently, the ferromagnetic contact induced spin splitting has been observed in F/QD/N devices in an InAs nanowire based QDs.[16]

We note that the problem of the current spin polarization in quantum dots coupled to ferromagnetic and normal leads has already been studied both theoretically[17–22] and experimentally;[23,24] however, this has mainly been carried out in the weak coupling regime. In this transport regime the effects related to the ferromagnetic-contact-induced exchange field are much suppressed and thereby the promising efficiency and functionality of the spin current injector and spin current amplifier discussed in this paper are missing.

Theoretical framework – Our model consists of a quantum dot strongly coupled to the left (L) ferromagnetic lead and weakly coupled to the right (R) nonmagnetic lead (see Fig. 1b). The strength of the tunnel couplings is described by the tunneling rates Γ_α (α = L, R), with $\Gamma_L = (\Gamma_{L\uparrow} + \Gamma_{L\downarrow})/2$. The spin polarization of the ferromagnet is taken into account by assuming different density of states for the spin-up (red) and spin-down (blue) subbands at the Fermi level, see Fig. 1b. For the circuit in Fig. 1c, the total electrostatic energy of the circuit is given by, $E_{tot} = E(n) - eN_R V$. Here, the potentials of the left and right electrodes were explicitly set to $V_L \to 0$ and $V_R \to -V$, and N_R denotes the number of particles on the right lead. The first term gives the energy of the quantum dot

$$E(n) = E_C(n - n_g)^2 - \frac{1}{2}\left(C_R V^2 + C_g V_g^2\right), \quad (1)$$

with n as the number of particles on the dot and C_α (V_α) is the capacitance (voltages) of the left, right and gate electrodes (α = L, R, g, respectively). $E_C = e^2/2C$ denotes the charging energy, with $C = C_L + C_R + C_g$. The parameter $n_g = (C_g V_g - C_R V)/|e|$ sets the number of electrons on the dot, with $e < 0$ denoting the electron charge and V the voltage drop on the dot.

At the quantum level, the Hamiltonian of the system can be written as a sum of three terms, $H = H_L + H_R + T$. Here, the left part (H_L) describes the dot and the more strongly coupled ferromagnetic lead,

$$H_L = H_{0L} + E_C(n - n_g)^2 + t_L \sum_{k\sigma}\left(c_{Lk\sigma}^\dagger d_\sigma + d_\sigma^\dagger c_{Lk\sigma}\right) + \text{cst.}, \quad (2)$$

and $H_R = H_{0R} - eN_R V$ describes the right electrode. In these equations n and N_α are particle number operators, $n = \sum_\sigma d_\sigma^\dagger d_\sigma$, and $N_\alpha = \sum_{k\sigma} c_{\alpha k\sigma}^\dagger c_{\alpha k\sigma}$, with $d_\sigma^\dagger$ creating a spin-σ electron on the dot and $c_{\alpha k\sigma}^\dagger$ being the creation operator of an electron of wave number k and spin σ in electrode α. The Hamiltonian $H_{0\alpha} = \sum_{k\sigma} \varepsilon_{\alpha k\sigma} c_{\alpha k\sigma}^\dagger c_{\alpha k\sigma}$ describes noninteracting electrons in the leads, while the last term of H_L describes tunneling between the electrons in the ferromagnetic lead and the dot, with t_L denoting the corresponding tunneling amplitude. Finally, the tunneling between the left and right subsystem is described by

$$T = t_R \sum_{k\sigma}\left(c_{Rk\sigma}^\dagger d_\sigma + d_\sigma^\dagger c_{Rk\sigma}\right), \quad (3)$$

with t_R the tunneling amplitude between the right lead and the dot.

Since the coupling of the dot is assumed to be much weaker to the right lead than to the left lead, we can perform a perturbative expansion in T. In leading order, we can express the current in the spin channel σ as

$$I_\sigma(V, V_g) = -\frac{|e|\Gamma_R}{\hbar}\int_{-\infty}^{\infty} d\omega A_\sigma(\omega, v_g - v)\left[f(\omega) - f(\omega - |e|V)\right], \quad (4)$$

where $v_g \equiv C_g V_g/|e|$ and $v = VC_R/|e|$ are the dimensionless gate and bias voltages, respectively (for the sign conventions, see Fig. 1) and $A_\sigma(\omega, n_g)$ is the spin dependent spectral function of the quantum dot coupled to the ferromagnetic lead (F/QD), as described by eqn (2). Note that the second argument of A determines the position of the dot level. Beside the dimensionless gate voltage, the level is also shifted by the bias voltage, which has a simple electrostatic reason (see Fig. 1c). This bias induced shift is important for the two terminal operations discussed below). The current is proportional to the tunneling rate to the right non-magnetic electrode, $\Gamma_R = 2\pi\rho_R t_R^2$, which is assumed to have a constant density of states, ρ_R, and $f(\omega)$ denotes the Fermi function. Eqn (4) implies that the spin polarization of the current, $P \equiv (I_\uparrow - I_\downarrow)/(I_\uparrow + I_\downarrow)$, is determined by the difference between the spectral functions, $A_\uparrow$ and $A_\downarrow$, in the energy window between the electrochemical potential of the left and right leads. As discussed in the following section, the spectral functions depend

strongly on the spin. Due to the ferromagnetic lead induced exchange field, the two Hubbard peaks get spin polarized with opposite spin orientations (see Fig. 1b). Large current polarizations can thus be achieved if the left and right chemical potentials are positioned next to one of these peaks.

In order to calculate the spectral function of the F/QD system, we employed the numerical renormalization group (NRG) method.[25–27] NRG is one of the most powerful tools to study transport through quantum dot structures and it reliably captures the ferromagnetic exchange-field induced spin splitting of the dot levels.[11,14] Note that the accurate non-perturbative NRG approach is essential to describe the problem. Neglecting the higher order correlations, the spin amplification is lost and the output current polarization can not exceed the F lead polarization.[15] The NRG calculations were performed for the single impurity Anderson model and the ferromagnet was modeled by flat subbands of different density of states for spin up and spin down electrons.[8,9] We assumed parameters typical for quantum dot structures and used $E_C/\Gamma_L = 10$ and a spin polarization of the ferromagnet of $p = 0.4$. Having determined the spectral functions, we used eqn (4) to compute the current. For the junction capacitance values, we assumed that $C_L/C_R = 2$ and $C_g/C_R = 0.1$, which are typical for semiconducting nanowire QDs.[16]

The maximum value of the injected current is given by $I_0 = |e|\Gamma_R/\hbar$. Taking typical semiconducting QD parameters,[28] $E_C = 5$ meV and $\Gamma_L = 0.5$ meV, and fulfilling the assumption of asymmetric couplings, *i.e.,* $\Gamma_R = \Gamma_L/10$, yields the maximum current in the range of $I_0 \approx 50$ nA. However, if E_C and Γ_L are larger, as it is in, for example, carbon nanotube QDs,[13,14] I_0 can be further enhanced. For molecule based QDs,[10] where E_C can be especially high ($E_C > 100$ meV), the maximum current can be even in the range of a few μAs.

Spectral functions – The results of our calculations for an unbiased dot ($V = 0$) are shown in Fig. 2. Panels (a) and (b) present the colorscale plots of the normalized zero-temperature spin-up (spin-down) spectral functions, $A_\uparrow(\omega, n_g)$ ($A_\downarrow(\omega, n_g)$), with ω denoting the energy measured from the Fermi level of the ferromagnet and n_g as the effective gate voltage. Upon increasing n_g, the dot's occupation changes from even to odd and then back to even. The change in charge occurs at $n_g \approx 1/2$ and $n_g \approx 3/2$, where the neighboring charge states with odd and even electrons become degenerate and the Hubbard resonances reach the Fermi energy, $\omega = 0$. The region around $n_g = 1$ is the Coulomb blockade region with an odd number of electrons (in our case $\langle n \rangle \approx 1$). Here, additional lines associated with Kondo correlations appear at $\omega \approx 0$. In this regime, the dot level is occupied by a single electron and the conduction electrons try to screen it through the Kondo effect. This would generate a resonance located normally at the Fermi level.[6,7] However, because of the ferromagnetic lead, an exchange field acts on the dot and splits and suppresses the Kondo resonance.[8,9] This results in smaller resonances occurring at energies corresponding to the magnitude of the exchange field. For the spin-up and spin-down orientations, the resonances shift in the opposite direction, as clearly seen in the cross-sections of the colorscale plots, Fig. 2c–e. The magnitude of the shift is equal to the effective ferromagnetic exchange field (B_{exch}) induced by Zeeman splitting, *i.e.,* $g\mu_B B_{exch}$. Importantly, due to correlation effects, this exchange field is not constant, but monotonously changes with n_g (see Fig. 2) and even *reverses* sign (see $n_g \approx 1$), as also demonstrated experimentally.[13,16] This effect forms the basis of the proposed electrical spin polarization control.

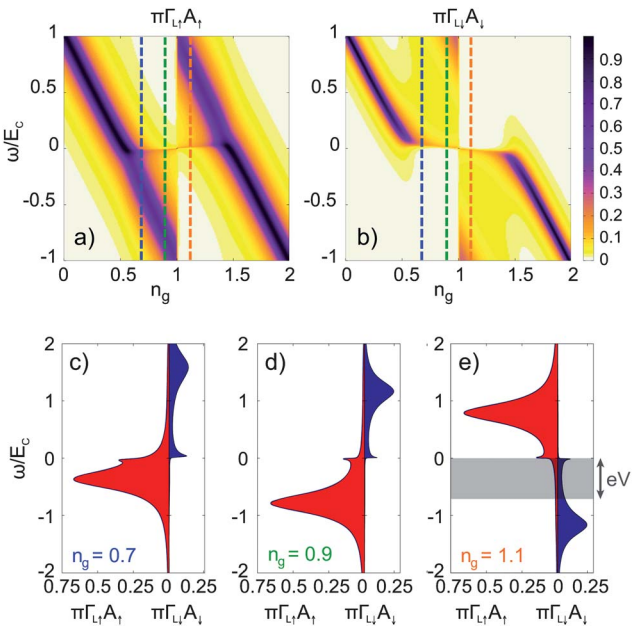

Fig. 2 The spectral functions of a quantum dot strongly coupled to the ferromagnetic lead calculated by NRG: panels (a) and (b) show the normalized zero-temperature spin-up ($A_\uparrow$) and spin-down ($A_\downarrow$) spectral functions as a function of energy (ω) and effective gate voltage (n_g). Panels (c), (d) and (e) show the cross-sections of the spectral function at the position of the dashed lines in (a) and (b) *i.e.,* at $n_g = 0.7$, 0.9, 1.1, respectively. As can be seen, the lower (occupied) Hubbard peak is spin-up polarized for $n_g < 1$, while its polarization changes sign for $n_g > 1$. In crossing $n_g = 1$ either by gate or bias voltage induced level shift ($-eV_d$), the sign of the current polarization can be reversed. The gray area in Panel (e) sketches the states contributing to the current at the bias voltage V. For the NRG calculation we used the parameters $p = 0.4$, $E_C = 0.1D$, $\Gamma_L = 0.01D$ and $D \equiv 1$ the half bandwidth.

Besides the splitting of the Kondo resonance, the ferromagnetic exchange field has another, even more dramatic consequence on the spectral functions: the Hubbard (resonance) peaks become almost fully spin-polarized. For $n_g < 1$ (see Fig. 2c,d) the lower/upper Hubbard peak is spin-up/spin-down polarized and, when the exchange field changes sign (for $n_g > 1$), the spin orientation of the Hubbard peaks is also reversed, see Fig. 2e. The proposed spin current injector is based on this robust polarization of the Hubbard peaks. If the current flows, for example, in the energy window shown by the gray stripe in Fig. 2e, it is strongly polarized due to the much larger contribution of the spin-down spectral density.

Three-terminal operation – The current flowing through the F/QD// N device and its spin polarization, P, are calculated by plugging the NRG spectral functions into eqn (4). The results obtained are shown in Fig. 3a and b. The colorscale plot of the current (Panel a) shows the expected Coulomb diamond behavior of the quantum dot. Focusing on the spin polarization (Panel b), the quantum dot acts as a polarization amplifier: high current polarizations are achieved, which could strongly exceed the polarization of the ferromagnetic lead ($p = 40\%$) and even become close to full polarization. The spin polarization is strongly enhanced in the extended parameter region, especially when close to the Coulomb peaks (*i.e.,* around $v_g = 1/2$, 3/2) or, for larger bias voltages, outside the Coulomb diamond. As a spin current source, these regions are also preferable, since the high polarization is combined with the high amplitude of the current. The sign of the spin

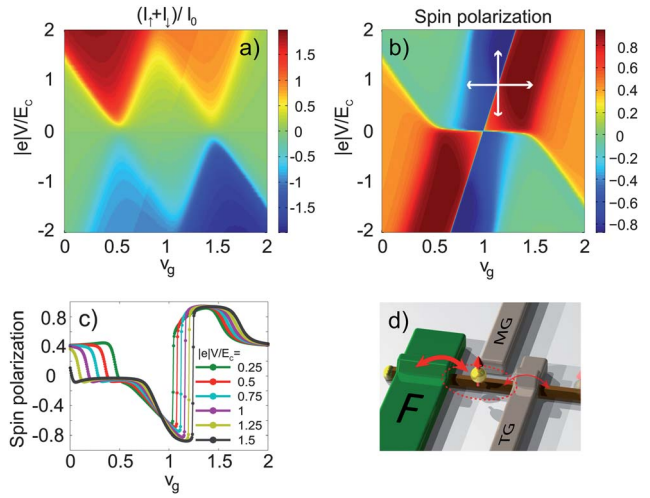

Fig. 3 The three terminal device operation: (a) total current $I = I_\uparrow + I_\downarrow$ in units of $I_0 = |e|\Gamma_R/\hbar$ as a function of the dimensionless gate voltage, $v_g = C_g V_g/|e|$, and applied bias voltage V. I/I_0 shows the expected Coulomb diamond behavior. (b) The spin polarization of the current for the same parameter range. As indicated by the white arrows, the spin polarization can be reversed either by modifying the level position or by changing the bias voltage. Panel (c) shows the spin polarization characteristics as a function of the dimensionless gate, v_g, for different bias voltages. Panel (d) shows a schematic of the proposed realization of the three terminal device: it consists of a nanowire (or a nanotube) strongly coupled to a ferromagnetic lead (F) with a top gate (TG) and a middle gate (MG). MG is used to change the level position of the dot, while TG defines the tunnel barrier with a weak coupling. The calculations were performed for the spectral functions shown in Fig. 2 with $\Gamma_R/\Gamma_L = 0.1$. The capacitance values were $C_L/C_R = 2$ and $C_g/C_R = 0.1$.

polarization is parallel to the lead polarization in the red region; however, it can have an opposite sign with a similarly high amplitude as well (blue region). This change of polarization is driven by the sign change of the local exchange field, which in turn induces a polarization change of the occupied Hubbard peak, see Fig. 2d and e.

Changing v_g alters the occupation by the gate voltage along the horizontal arrow in Fig. 3b, *i.e.*, the spin polarization of the current is reversed. This makes the F/QD//N device an efficient gate-controlled spin current source: the polarization is switchable by the gate electrode, which can be modulated really fast (over 10 GHz as shown by Nowack *et al.*[29]). The speed of the switch can also be limited by Γ_L, which is, however, typically also in the GHz range or above, depending on the type of device.

As shown in Fig. 3c, the switching of the spin polarization takes place for a wide range of applied bias voltages with relatively high up and down polarizations ($P \approx 90\%$). Fig. 3d shows a proposed device geometry for the realization of the gate-controlled spin current source. A ferromagnetic lead couples strongly to a nanowire (or a carbon nanotube), a middle gate (MG) tunes the dot level, while a top gate (TG) defines the tunnel barrier with weak coupling and the rest of the nanowire serves as a normal lead. Since the ferromagnetic lead-induced local exchange field, its sign change and the fabrication of side and top gates have all been demonstrated in carbon nanotubes[13,14] and nanowire[16]-based structures, the realization of the proposal is within reach with state-of-the-art nanofabrication techniques. Besides the large amplification and the fast gate control, this geometry could solve the demanding issues of spin injection into carbon nanotubes or nanowires, *i.e.*, the fabrication of proper tunnel barriers at the interface[1] as coupling a ferromagnetic lead strongly to these nanoobjects is much simpler and it induces a ferromagnetic proximity effect that gives rise to a highly polarized spin current, which could be injected through the other weakly coupled barrier of the quantum dot.

Two-terminal operation – The F/QD//N system can be also used as a two-terminal spin injector, where the presence of a gate electrode is not required. As can be seen in Fig. 3b, the value of v_g, where the spin polarization reversal takes place, depends on the bias voltage. The reason for this can be understood based on the simple circuit model shown in Fig. 1c: the applied bias (V) also shifts the dot level with the value of $eV_d = -eVC_R/C$. As a consequence, the spin polarization can also be changed just by varying the bias voltage, *e.g.*, along the vertical arrow shown in Fig. 3b. We call this the two terminal operation, since it does not require the change of v_g, *i.e.*, a change of the gate voltage to reverse the spin polarization. As demonstrated in Fig. 4, the spin polarization as a function of the bias voltage reverses over a wide range of v_g. Moreover, the polarization reversal with highly polarized spin-up and spin-down currents ($|P| > 0.6$) can be generated even with rather small bias voltages, $|V| < 0.4E_C/|e|$ (see the green curve in Fig. 4a).

The two terminal operation allows the realization of the spin injector using molecular QD systems, such as modified buckyballs (see Fig. 4b),[30] where gates are not necessarily available. Due to the much larger energy scales of molecular quantum dots (charging energies in the order of tens–hundreds of meV), these devices could operate close to room temperature. Furthermore, molecular quantum dots also allow for the down-scaling of the spin injector and support a much faster operation and a larger value of the injected current too. In addition, molecules could also form monolayers; thus, the output current of the spin injector could be enhanced significantly by the contribution of parallel molecular quantum dots.

Finally, let us comment on the presence of a finite temperature, which has been neglected so far. Since the injected current is almost entirely associated with the Hubbard peaks, the polarization amplification is effective as long as $T \ll E_C$. However, the polarization switch is smeared out by a finite temperature and an effective exchange field, $B_{exch} \gg T$, is required to polarize the dot spin and reach close to maximum polarizations. While, for quantum dots, this may imply below Kelvin device temperatures, for a molecular device these conditions can be relatively easily satisfied and even a room temperature operation may be possible.

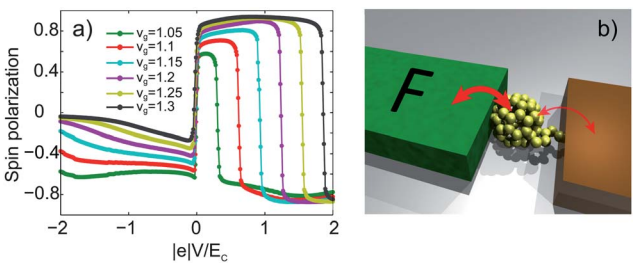

Fig. 4 The two terminal device operation: (a) shows the spin polarization as a function of the bias voltage for different values of v_g. These are the cross-sections from Fig. 3b. The spin polarization highly exceeds the polarization of the ferromagnetic lead and it reverses sign for positive bias voltages. Panel (b) presents the proposed realization with asymmetrically coupled molecules.

Conclusions – In conclusion, we presented a proposal for an efficient spin injector, which is based on a quantum dot strongly coupled to a ferromagnetic lead and weakly coupled to a normal one. The proposed spin injector has several advantageous properties: (i) if the ferromagnet–dot coupling is substantially larger than the normal-dot coupling then the output current gets almost fully polarized, since the dot strongly amplifies the spin polarization of the ferromagnetic lead. (ii) The polarization of the current can be reversed purely electrically by a small change in the gate voltage. The spin switch is thus induced *without* modifying the polarization of the ferromagnetic lead, which allows an extremely fast polarization switching. (iii) The quantum dot based spin injector can also operate in a two-terminal configuration, where the current polarization is reversed by simply changing the applied bias voltage. This allows its implementation in molecular quantum dot systems as well. (iv) As a molecular electronics device, the proposed injector would allow the injection of relatively large polarized currents into other nanoscale objects and could also be integrated into more complex nanodevices.

We emphasize again that the basic ingredients of the proposal have already been demonstrated experimentally in various nanoscale quantum dot systems, such as carbon nanotubes, semiconductor nanowires/dots and molecular quantum dots; thus, the realization should be feasible with state-of-the-art experimental techniques.

We acknowledge support from EU ERC CooPairEnt 258789, FP7 SE2ND 271554, the EU-NKTH GEOMDISS project, Hungarian grant No. OTKA CNK80991, K73361, TÁMOP-4.2.2.B-10/1–2010-0009 and EU ERG-239223. I.W. acknowledges support from the Polish Ministry of Science and Higher Education through a 'Iuventus Plus' research project for the years 2010–2011, the Alexander von Humboldt Foundation and EU grant No. CIG-303689. G.Z. acknowledges support from the DFG.

References

1 I. Žutić, J. Fabian and S. Das Sarma, *Rev. Mod. Phys.*, 2004, **76**, 323.
2 P. C. van Son, H. van Kempen and P. Wyder, *Phys. Rev. Lett.*, 1987, **58**, 2271.
3 G. Schmidt, D. Ferrand, L. W. Molenkamp, A. T. Filip and B. J. van Wees, *Phys. Rev. B: Condens. Matter*, 2000, **62**, R4790.
4 G. M. Jagadeesh, S. Moodera and T. S. Santos, *Phys. Today*, 2010, **63**, 46.
5 R. Meservey and P. M. Tedrow, *Phys. Rep.*, 1994, **238**, 173.
6 D. Goldhaber-Gordon, H. Shtrikman, D. Mahalu, D. Abusch-Magder, U. Meirav and M. A. Kastner, *Nature*, 1998, **391**, 156.
7 S. M. Cronenwett, T. H. Oosterkamp and L. P. Kouwenhoven, *Science*, 1998, **281**, 5376.
8 J. Martinek, Y. Utsumi, H. Imamura, J. Barnaś, S. Maekawa, J. König and G. Schön, *Phys. Rev. Lett.*, 2003, **91**, 127203.
9 M.-S. Choi, D. Sanches and R. Lopez, *Phys. Rev. Lett.*, 2004, **92**, 056601.
10 A. N. Pasupathy, R. C. Bialczak, J. Martinek, J. E. Grose, L. A. K. Donev, P. L. McEuen and D. C. Ralph, *Science*, 2004, **306**, 86.
11 J. Martinek, M. Sindel, L. Borda, J. Barnaś, R. Bulla, J. König, G. Schön, S. Maekawa and J. von Delft, *Phys. Rev. B: Condens. Matter Mater. Phys.*, 2005, **72**, 121302(R).
12 K. Hamaya, M. Kitabatake, K. Shibata, M. Jung, M. Kawamura, K. Hirakawa, T. Machida, T. Taniyama, S. Ishida and Y. Arakawa, *Appl. Phys. Lett.*, 2007, **91**, 232105.
13 J. R. Hauptmann, J. Paaske and P. E. Lindelof, *Nat. Phys.*, 2008, **4**, 373.
14 M. Gaass, A. Hüttel, K. Kang, I. Weymann, J. von Delft and Ch. Strunk, *Phys. Rev. Lett.*, 2011, **107**, 176808.
15 Z. G. Zhu, *Phys. Lett. A*, 2008, **372**, 695.
16 L. Hofstetter, A. Geresdi, M. Aagesen, J. Nygard, C. Schönenberger and S. Csonka, *Phys. Rev. Lett.*, 2010, **104**, 246804.
17 J. Wang, K. S. Chan and D. Y. Xing, *Phys. Rev. B: Condens. Matter Mater. Phys.*, 2005, **72**, 115311.
18 I. Weymann and J. Barnaś, *Phys. Rev. B: Condens. Matter Mater. Phys.*, 2006, **73**, 205309.
19 H. Dalgleish and G. Kirczenow, *Phys. Rev. B: Condens. Matter Mater. Phys.*, 2006, **73**, 235436.
20 F. M. Souza, J. C. Egues and A. P. Jauho, *Phys. Rev. B: Condens. Matter Mater. Phys.*, 2007, **75**, 165303.
21 E. Perfetto, G. Stefanucci and M. Cini, *Phys. Rev. B: Condens. Matter Mater. Phys.*, 2008, **78**, 155301.
22 J. Barnaś and I. Weymann, *J. Phys.: Condens. Matter*, 2008, **20**, 423202.
23 A. ChristopherMerchant and Nina Markovic, *Phys. Rev. Lett.*, 2008, **100**, 156601.
24 K. Hamaya, M. Kitabatake, K. Shibata, M. Jung, S. Ishida, T. Taniyama, K. Hirakawa, Y. Arakawa and T. Machida, *Phys. Rev. Lett.*, 2009, **102**, 236806.
25 K. G. Wilson, *Rev. Mod. Phys.*, 1975, **47**, 773.
26 R. Bulla, T. A. Costi and T. Pruschke, *Rev. Mod. Phys.*, 2008, **80**, 395.
27 For a description of the code, see: O. Legeza, C. P. Moca, A. I. Tóth, I. Weymann and G. Zaránd, arXiv:0809.3143 (2008); the code is available at, http://www.phy.bme.hu/~dmnrg/.
28 L. Hofstetter, S. Csonka, J. Nygard and C. Schönenberger, *Nature*, 2009, **461**, 960.
29 K. C. Nowack, F. H. L. Koppens, Yu. V. Nazarov and L. M. K. Vandersypen, *Science*, 2007, **318**, 1430.
30 L. Grüter, F. Cheng, T. T. Heikkilä, M. T. Gonzalez, F. Diederich, Ch. Schönenberger and M. Calame, *Nanotechnology*, 2005, **16**, 2143.